Author's version of the manuscript accepted for publication in *Plant and Soil*
The final publication is available at Springer via http://dx.doi.org/10.1007/s11104-015-2673-4
Delory et al. (2016). *Plant and Soil*, 398, 351-365.

archiDART: an R package for the automated computation of plant root architectural traits

Benjamin M. Delory [a], Caroline Baudson [a], Yves Brostaux [b], Guillaume Lobet [c], Patrick du Jardin [a], Loïc Pagès [d], Pierre Delaplace [a, *]

[a] University of Liège – Gembloux Agro-Bio Tech. Plant Biology, Passage des Déportés, 2, B-5030 Gembloux, Belgium

[b] University of Liège – Gembloux Agro-Bio Tech. Applied Statistics, Computer Science and Modeling, Passage des Déportés, 2, B-5030 Gembloux, Belgium

[c] University of Liège, Laboratory of Plant Physiology, PhytoSYSTEMS, Boulevard du Rectorat, 27, B-4000, Liège, Belgium

[d] INRA, Centre PACA, UR 1115 PSH, Domaine Saint-Paul, Site Agroparc, 84914 Avignon cedex 9, France

[*]Corresponding author: Pierre Delaplace

Address: University of Liège – Gembloux Agro-Bio Tech. Plant Biology, Passage des Déportés, 2, B-5030 Gembloux, Belgium

Email: Pierre.Delaplace@ulg.ac.be

Phone: +32-81-62.24.50

Acknowledgements

Delory B.M. (Research Fellow) and Lobet G. (Postdoctoral Researcher) are financially supported by the Belgian National Fund for Scientific Research. The authors would like to thank Jacques Le Bot (INRA, Centre PACA, UR 1115 PSH) for providing the vectorized root system of the tomato plant used in this paper, and Pierre Tocquin (University of Liège, PhytoSYSTEMS) and three anonymous reviewers for their helpful comments on the manuscript.

Keywords

Plant root system architecture; Data Analysis of Root Tracings (DART); Root System Markup Language (RSML); 2D dynamic analysis; root trait.

Abstract

Background and Aims

In order to analyse root system architectures (RSAs) from captured images, a variety of manual (e.g. Data Analysis of Root Tracings, DART), semi-automated and fully automated software packages have been developed. These tools offer complementary approaches to study RSAs and the use of the Root System Markup Language (RSML) to store RSA data makes the comparison of measurements obtained with different (semi-) automated root imaging platforms easier. The throughput of the data analysis process using exported RSA data, however, should benefit greatly from batch analysis in a generic data analysis environment (R software).

Methods

We developed an R package (archiDART) with five functions. It computes global RSA traits, root growth rates, root growth directions and trajectories, and lateral root distribution from DART-generated and/or RSML files. It also has specific plotting functions designed to visualise the dynamics of root system growth.

Results

The results demonstrated the ability of the package's functions to compute relevant traits for three contrasted RSAs (*Brachypodium distachyon* [L.] P. Beauv., *Hevea brasiliensis* Müll. Arg. and *Solanum lycopersicum* L.).

Conclusions

This work extends the DART software package and other image analysis tools supporting the RSML format, enabling users to easily calculate a number of RSA traits in a generic data analysis environment.

Introduction

As water and nutrients are resources characterised by a heterogeneous spatial and temporal distribution in the soil, the selection of plants able to develop a root system architecture (RSA) that optimizes water and nutrient uptake in various growing conditions has been shown to be an important target for crop improvement in terms of sustainable agriculture (Lynch 1995; de Dorlodot et al. 2007; Den Herder et al. 2010; Meister et al. 2014). In this context, linking genotypes and environmental conditions to phenotypes requires the use of high-throughput plant phenotyping platforms that allow a quantitative analysis of a large number of plants on which an increasing number of traits can be accurately measured (Cobb et al. 2013; Fiorani and Schurr 2013). Due to its complexity and belowground localisation, however, phenotyping a root system is challenging and numerous tools are being developed to address this difficulty. These tools are part of a processing chain that consists of three main steps: (1) high-resolution imaging of excavated (2D) or undisturbed (2D or 3D) root systems, (2) recognition of the relevant biological structures in the captured images (Zhu et al. 2011), and (3) calculation of static and dynamic features that describe the RSA either locally (for an individual root, a specific root class, etc.) or globally (at the whole root system scale) (de Dorlodot et al. 2007; Clark et al. 2011; Nagel et al. 2012). Using high-resolution images acquired with light or confocal microscopes (Wells et al. 2012; Slovak et al. 2014), flatbed scanners (Pagès 2014), digital cameras (Le Marié et al. 2014; Mathieu et al. 2015) or non-invasive 3D techniques such as X-ray computed tomography and magnetic resonance imaging (Zhu et al. 2011), software packages can be used for the detection of roots on captured images prior to the calculation of relevant RSA traits. Depending on the level of interaction between the user and the imaging software, root detection can be performed manually (Le Bot et al. 2010), semi-automatically (Lobet et al. 2011; Clark et al. 2013; Pound et al. 2013) or fully automatically (French et al. 2009; Iyer-Pascuzzi et al. 2010; Wells et al. 2012; Diener et al. 2013; Kumar et al. 2014; Leitner et al. 2014; Pace et al. 2014; Slovak et al. 2014; Bucksch et al. 2014; Cai et al. 2015). The use of a manual tracing software tool like Data Analysis of Root Tracings (DART) is well suited for the 2D analysis of mature root systems with a high level of root overlaps or for rhizotron images, but it is not suitable in a high-throughput phenotyping context for which scientists will prefer automated or semi-automated tracing tools. As a consequence of the variety of 2D image analysis software solutions dedicated to the analysis of RSAs [listed in the Plant Image Analysis Database, (Lobet et al. 2013)], the comparison of measurements acquired with different platforms is often difficult, mainly because these platforms do not compute the same RSA traits and the stored RSA data do not share a common structure. In order to partly solve this problem, the Root System Markup Language (RSML) has been recently introduced as a convenient way to store and exchange RSA data in a standardized format (Lobet et al. 2015). At the time of writing,

a RSML support has been implemented in two semi-automated (SmartRoot and RootNav) and three automated (RootTrace, RhizoScan and RootSystemAnalyser) 2D root image analysis software tools. As manual, semi-automated and fully automated root tracing solutions offer complementary approaches to study RSAs and generate large datasets from which relevant RSA traits can be calculated, it would be of great interest to develop a tool allowing the batch analysis of DART-generated and/or RSML files using automated procedures in a generic data analysis environment that allows easy access to the calculated RSA traits for further statistical analyses (Table 1). In order to achieve this goal, we developed an R package (**archiDART**) for the computation of global RSA traits (root length, root number, etc.) at each observation date, root growth directions and trajectories (branching and root tip angles, root curvature), and lateral root length and density distribution from DART and RSML files (Delory et al. 2015). The package also enables the dynamics of root system growth and local root growth rate variations to be visually assessed using specific plotting and mapping functions. In this paper, our objective was to present the main functionalities of archiDART and demonstrate the added value of this package using contrasted RSAs.

Materials and Methods

In order to illustrate the functionalities of the R package archiDART, we performed a quantitative root system architecture analysis of a model cereal (*Brachypodium distachyon* [L.] P. Beauv.) and two dicotyledonous plant species (*Hevea brasiliensis* Müll. Arg. and *Solanum lycopersicum* L.) produced under various growing conditions and we focused our analysis on selected root traits that were particularly relevant for each plant species.

Example 1: Time series images of *Brachypodium* plantlets exposed to rhizobacterial volatiles *in vitro*

In order to show the impact of volatile compounds emitted by plant growth-promoting rhizobacteria (PGPR) commonly found in the plant's rhizosphere on the RSA of a model cereal, eight root systems of *B. distachyon* plantlets were produced *in vitro* in square petri dishes on a Hoagland medium and were either co-cultivated with one PGPR strain (*Bacillus pumilus* C26, *Bacillus subtilis* AP305-GB03 or *Enterobacter cloaceae* AP12-JM22) or cultivated alone following the protocol described by Delaplace et al. (2015), except that the photoperiod used in the growth chamber was 16 h/8 h – L/D and the lateral roots were detected without setting a minimal length threshold. Monitoring the RSA of each plantlet started at the beginning of the experiment (day 0) and was performed by scanning each root system at 400 dpi every 24 h for 11 days. At the end of the experiment (day 11), a single composite image of each root system was constructed with Adobe Photoshop 7.0.1 (Adobe Systems

Incorporated, San Jose, CA, USA). In order to facilitate the vectorization with DART, the new root segments that appeared at each observation date were drawn with a specific colour.

Example 2: Time series images of the root system of a rubber tree growing in a rhizotron

The root system of this rubber tree species was produced in a vertical root observation box filled with 2 mm-sieved vermiculite. The development of the root system was monitored every 2 days by drawing the new growth increments on a transparent plastic sheet using a unique colour for each observation date. The RSA used in this work was that of a 37-day-old *H. brasiliensis* seedling (Thaler and Pagès 1996a).

Example 3: Time series images of a tomato root system produced hydroponically

As a third example, we used the root system of a tomato plant produced hydroponically in a horizontal flat box, as described by Le Bot et al. (2010). Images of the entire root system were taken every 24 h using a digital camera. The RSA used in this work was that of a 28-day-old tomato plant.

RSA input data

Two types of RSA input data can be used to compute RSA traits with the R package archiDART (Table 1): (1) the files exported by Data Analysis of Root Tracings (DART) (Le Bot et al. 2010) and (2) RSA data encoded with the Root System Markup Language (RSML) (Lobet et al. 2015). Although DART-generated and RSML files do not share a common structure, the functions of our R package use the file extensions to discriminate between these two file types and compute RSA traits for each independently, allowing the batch analysis of DART-generated and RSML files in a single operation.

In this paper, the images showing the RSA of each plant species were processed with DART and the files containing topological (file extension: .rac), temporal (file extension: .tps) and spatial (file extension: .lie) attributes were saved into a specific folder for each plant species after the manual vectorization of each root system. The RSAs were then analysed with the archiDART 1.1 package (Delory et al. 2015) using the 3.2.0 version of R statistical software (R Core Team 2015).

Overview of the package's functions

The archiDART package (version 1.1) has five functions (*archidraw*, *archigrow*, *architect*, *latdist* and *trajectory*) that allow the batch processing of many root systems by simply knowing (1) the path(s) to the folder(s) containing the DART-generated and/or the RSML files exported by another root imaging software tool supporting this file format, (2) the unit of length and unit of time that should be used by the functions in order to perform the calculations and express the results, and (3) the resolution of the images used to vectorize the root systems (if images were acquired with a flatbed scanner; resolution is expressed in dots/inch) or the ratio between the length of a reference object located on the image expressed in pixels and the actual length of the same object expressed in inches (if images were acquired with a digital camera) (Delory et al. 2015). An overview of the required files, returned R objects and calculated RSA traits for each R function of the package is shown in Table 1. A full description of the values taken by each function is in the documentation files provided with the R package (http://cran.r-project.org/package=archiDART).

The graphical functions *archidraw* and *archigrow* allow the X-Y plotting of each vectorized root system for selected observation dates. They both use the generic X-Y plotting functions of the R package 'graphics' (R Core Team 2015) to plot the vectorization results of many root systems in a single operation. Whereas *archidraw* is a plotting function that allows the graphical representation of a root system with a colour code depending on the observation date at which a link is seen for the first time, *archigrow* allows both the exportation of growth rate matrices and the X-Y plotting of vectorized root systems with a colour code depending on the growth rate value of each link constituting the vectorized root systems. The *archigrow* function computes root growth rates following the method described in Table 2. Using these functions, the user can easily customize the graphical outputs by setting additional graphical parameters.

The *architect* function was designed for the one-step calculation of a number of integrated RSA traits in order to provide an overall description of entire root systems at each observation date (Table 1). Root lengths, root numbers and lateral root densities are computed by the *architect* function according to the methods described in Table 2. In addition to these parameters, the secondary root distribution along a first-order root can also be studied with *architect*. To do so, one has to delimit zones along the first-order root before running the function using the rootdiv argument. The total secondary root length, the total number of secondary roots and the secondary root density will then be computed for each zone on the first-order root. The calculated RSA parameters are stored in a data frame that can easily be used for subsequent statistical analyses with R or other statistical software.

The purpose of the *latdist* function is to describe lateral root length and density distribution along each mother root of a vectorized root system (Table 2). To do so, the function use the distance between each branching point to the parent root base (DBase, Fig. 1a) in order to select the daughter roots to be used for calculating local lateral root lengths and densities along each parent root. Using the *latdist* function comprises two main steps. First, the function selects the points along the parent roots on which the calculation of RSA parameters should be performed. Depending on user choice, these points can be selected with or without linear interpolation. The use of interpolated points allows a more continuous evaluation of the lateral root length and density distribution on each parent root. Lateral root density and a total lateral root length are then calculated at intervals of a length defined by the experimenter and centred on each selected point. At the end of the calculation process, the results are stored in a list, giving easy access to the computed RSA traits for each mother root of each analysed root system. A second algorithm for measuring the inter-branch distances was also incorporated to *latdist* (Table 2).

With regard to the importance of root growth directions and trajectories in RSA, the *trajectory* function was designed to calculate root growth angle (basal branching and root tip angles), orientation and tortuosity, as well as statistical parameters (mean and standard deviation) that describe the curvature of each root of a vectorized root system. These RSA traits are computed by the *trajectory* function following the methods described in Table 2. As the orientation of the vectorized root system can be different from that of the natural plant root system depending on the device used to acquire root images, one can specify an angle value that will be used by the function to rotate the vectorized root system clockwise before calculating the RSA parameters. Because the angle values computed by *trajectory* depend on the initial values of l.brangle and l.tipangle (Table 2), these must be carefully chosen before running the function and will be notably linked to the plant species studied. The curvature of a root can be evaluated by its tortuosity. In addition, *trajectory* also allows the computation of statistical parameters (mean and standard deviation) that characterise the distribution of local angles measured at selected points linearly interpolated along a root. The method used by *trajectory* to calculate local angles on a root is very similar to that used in RootTrace (French et al. 2009) and comprises three main steps. First, the function will position equidistantly spaced points along each root constituting a vectorized root system. The distance between the interpolated points (l.curv) is set by the user before running the *latdist* function. Second, the angles (θ_{ij}) between the direction vectors ($\overrightarrow{H_{IJ}}$) of successive links along each root are calculated (Fig. 1d). As pointed out by French et al. (2009), a high θ_{ij} value is associated with a pronounced local curvature. The mean and standard deviation of the calculated angles are then determined for each root. As the user-defined distance between the interpolated points (l.curv) affects the computed local angles between successive direction vectors, the initial value of this

parameter should be carefully chosen by the experimenter before carrying out the function in order to best fit the RSA of the considered plant.

Results

archidraw: X-Y plotting of vectorized root systems

In order to qualitatively compare several RSA across time series experiments and export the vectorized root systems as high-resolution images, we developed an R function allowing the X-Y plotting of each vectorized root system for selected observation dates. As an example, we used *archidraw* to plot the RSA of a 12-day-old *B. distachyon* plantlet produced *in vitro* and exposed to the volatiles emitted by *B. subtilis* AP305-GB03 (Example 1, Fig. 2a), the RSA of a 37-day-old rubber tree produced in a vertical rhizotron (Example 2, Fig. 2b) and part of the RSA of a 28-day-old tomato plant produced hydroponically in a horizontal flat box (Example 3, Fig. 2c). The last-mentioned RSA was plotted with a specific colour for each observation date.

archigrow: computing growth rate matrices and X-Y plotting of vectorized root systems

As the graphical outputs exported by *archidraw* did not allow the visual detection of the root system parts that were characterised by high or low growth rate values, we developed a second mapping function (*archigrow*) allowing both the exportation of growth rate matrices and the X-Y plotting of vectorized root systems for selected observation dates with a colour code depending on the growth rate value of each link constituting the vectorized root systems. Such a tool could be particularly useful for rapidly screening local growth rate variations between analysed root systems. As an example, we used *archigrow* to study the growth rate variations between four root systems of *B. distachyon* plantlets that were or not exposed to rhizobacterial-emitted volatiles (Example 1). The results showed that plants exposed to bacterial volatiles were characterised by higher growth rate values for the primary root and the first-order lateral roots (Fig. 3).

architect: computing parameters describing the global RSA

In order to quantitatively compare the architecture of many root systems, it is often useful to start the data analysis process by calculating the RSA traits that provide a global description of each root system. In this way, *architect* is an R function performing a one-step calculation of common RSA traits for each analysed root system at each observation date. To illustrate this R function, we used *architect* on the DART files associated with the *B. distachyon* root systems (Example 1) and we plotted the results for three RSA parameters showing contrasted

222 results between experimental treatments (Fig. 4). The use of *architect* allowed a rapid analysis of the effects of
223 rhizobacterial volatiles on the RSA of *B. distachyon* plantlets. As shown in the figures, the root system of plants
224 exposed to rhizobacterial volatiles had a higher growth rate (Fig. 4a), a higher number of lateral roots (Fig. 4b)
225 and a greater length of first-order lateral roots (Fig. 4c) than the control plants at the end of the experiment. These
226 results confirm the growth rate variations observed between experimental treatments using the mapping function
227 *archigrow* (Fig. 3). Both *architect* and *archigrow* can be used to compare the growth kinetics of root systems but
228 these two functions will not have the same spatial resolution when computing root growth rates. Whereas *architect*
229 allows the computation of growth rates for the entire root system or for each branching order at each observation
230 date, the growth rate matrices and the graphical outputs exported by *archigrow* allow an analysis of the entire root
231 system growth with a far higher spatial resolution because a 'root by root' analysis can be performed.
232
233 *latdist*: computing lateral root length and density distribution
234 As DART is a software package that can provide length and topological information for each root of a vectorized
235 root system (Le Bot et al. 2010), notably via a distance calculated between each branching point and the
236 corresponding parent root base (DBase, Fig. 1a), an algorithm that could convert this information into lateral root
237 length and density distribution on each mother root would be a valuable tool for RSA analysis. In order to illustrate
238 the outputs calculated by *latdist*, we used it on four root systems of *B. distachyon* plantlets that were or were not
239 exposed to rhizobacterial volatiles (Example 1, Fig. 5), as well as on the root system of a rubber tree that had
240 shown periodicity in lateral root development (Example 2, Fig. 6) (Thaler and Pagès 1996b). For clarity reasons,
241 the results plotted in Fig. 5 and 6 show only the evolution of lateral root density, the lateral root length and the
242 distance between neighbouring lateral roots for the primary root. For *B. distachyon*, a maximum lateral root density
243 of 11-13 roots/cm was reached in a zone localized between 1.2 and 1.8 cm from the primary root base and no clear
244 difference emerged when the four root systems were compared for that variable (Fig. 5, a-d) or for the distances
245 between neighbouring lateral roots (Fig. 5, i-l). As for the total length of the first-order lateral roots, this showed
246 a maximum value localized between 1.1 and 1.6 cm, which parallels the results obtained for lateral root density
247 distribution. When the results were compared for that primary root zone, it was evident that total secondary root
248 length was lower for the control plant (2.2 cm of secondary roots/cm of primary root) than for the plants exposed
249 to rhizobacterial volatiles (5.1-5.6 cm of secondary roots/cm of primary root), confirming that the lateral root
250 elongation rate was lower for the unexposed plant (Fig. 5, e-h). In a second example, we tested the ability of *latdist*
251 to detect a periodic pattern in the lateral root development of a rubber tree, as described by Thaler and Pagès

(1996b). Three first-order lateral root density maxima were visually detected along the taproot of the rubber tree (Fig. 6a). The first maximum (9 roots/cm) was located between 0.7 and 1 cm from the taproot base. This local maximum was associated with secondary roots that started to develop early (Le Roux and Pagès 1994). Two additional local maxima associated with acropetal first-order lateral roots were also detected at 6.9 (8 roots/cm) and 27.7 cm (8 roots/cm) from the taproot base. The secondary root length distribution along the taproot paralleled the lateral root density distribution with high and low lateral root lengths calculated in zones with high or low branching densities, respectively (Fig. 6b). The use of the *archigrow* function to study the evolution of lateral root vigour along the taproot showed that highly branched areas with high lateral root growth rates alternated with poorly branched areas characterised by low lateral root growth rates (Fig. 7). Taken together, these results demonstrate the ability of *latdist* and *archigrow* to detect a periodic developmental process in a rubber tree for first-order lateral root emergence and elongation, as previously demonstrated by Thaler and Pagès (1996b).

trajectory: computing RSA traits describing root growth directions and trajectories

The *trajectory* R function was designed for calculating root traits that describe root growth directions and trajectories. To illustrate some outputs of *trajectory*, we used the function on the DART files associated with the root system of a 37-day-old rubber tree (Example 2). First, we compared the branching angles of the main root types identified by Le Roux and Pagès (1994) (Fig. 8a). The results showed that the branching angles of early and acropetal secondary roots had median values of 59.2° and 70.8°, respectively. By contrast, the tertiary roots had a higher median value (82.3°) and greater variability than the branching angles measured for the secondary roots. Second, we studied the potential of *trajectory* to follow the root tip angle of selected roots growing in a vertical rhizotron for 34 days (Fig. 8b). For clarity reasons, in the figure the evolution of the root tip angle during the cultivation period is shown only for the taproot, the two longest early secondary roots and the two longest acropetal secondary roots. The results showed that the taproot grew almost vertically with a root tip angle of 4.3° ± 4.5° (mean ± sd). Compared with the acropetal secondary roots, the two analysed early secondary roots seem to grow with a steeper root tip angle. It can also be seen that one of the acropetal secondary roots grew with a negative gravitropism at the end of the experiment because its registered root tip angle at the last observation date was greater than 90° (92.7°).

Discussion

In this paper, we presented five functions of an R package (archiDART, version 1.1) designed for the automated computation of RSA traits from data exported by manual (DART) or semi- and fully automated root image analysis platforms that have been implemented with a Root System Markup Language (RSML) support. Considering the increasing number of root image analysis tools, the RSML was introduced as a convenient way to store and exchange RSA data between imaging software tools (Lobet et al. 2015; Lobet 2015). In order to allow the analysis of RSML files with the archiDART package, an import function has been implemented in *architect*, *archidraw*, *latdist* and *trajectory*. Briefly, this function converts the RSA data encoded in each RSML file into data frames possessing the same structure as the files generated by DART before calculating the RSA traits. This import function allows the processing of RSML files and extends the use of the archiDART package to RSA data that were exported with root imaging software tools supporting this file format (Fig. 9). Therefore, as the functions of the archiDART package can use the spatial and topological information stored in both DART and RSML files to compute relevant RSA traits, this tool allows the comparison of root systems skeletonized with different root tracing solutions and complements these software packages with the possibility to compute new RSA traits. When coupled with DART or root imaging software tools supporting the RSML format, the archiDART package improves the RSA analysis process by allowing the batch analysis of many root systems and the computation of relevant parameters aimed at describing each analysed RSA at both a global and a local scale. To date, the package's functionalities include the computation of RSA traits and graphical outputs that allow (1) a global and dynamic analysis of root system growth (*architect, archidraw*), (2) an efficient description and mapping of growth rate variations between components of a single or many root systems (*archigrow*), (3) a detailed analysis of lateral root length and density distribution along the mother roots of each analysed root system (*latdist*), and (4) a comprehensive analysis of root growth directions and trajectories via the calculation of branching and root tip angles, as well as parameters characterising root curvature (*trajectory*).

The choice of a root tracing solution for the analysis of root system architectures is conditioned by the quality and the number of root images, the level of automation required by the experimenter, as well as the RSA traits that should be measured on captured images. Although most root imaging platforms deal with root number and root length measurements, other RSA traits that are computed by a limited number of platforms can be more relevant to analyse in certain situations. Among all the parameters that can be calculated by the archiDART package, lateral root length and density distribution are two important RSA traits for at least two reasons. First, as roots compete with each other for shared internal resources, the optimal number of lateral roots will be related to the balance

between their metabolic costs and the need for root development and resource acquisition (Lynch 2013). Second, as mobile resources (e.g., water and nitrates) are more efficiently taken up by long but dispersed laterals and immobile resources (e.g., phosphorus) are more efficiently acquired by fine but dense laterals, these RSA features will determine the balance between mobile and immobile resource uptake (López-Bucio et al. 2003; Malamy 2005; Lynch 2013). In addition, as resource acquisition by plant roots is challenged by a heterogeneous spatial and temporal distribution of water and nutrients in the soil (Lynch 1995; Giehl et al. 2014), root growth direction and trajectories also play an important role in the development of RSA, but only a few root imaging platforms are able to compute such traits (Lobet et al. 2013). Among the possible parameters aimed at describing RSA, root growth angles are of major importance in resource foraging and depend on root type, edaphic conditions and genotype (Rich and Watt 2013; Wu et al. 2014). As shallow and steep root growth angles are associated with topsoil and deep foraging strategies, respectively, root growth angles will condition the soil layers that will be explored by plant roots (Forde and Lorenzo 2001; Lynch 2013; Uga et al. 2013). Root growth direction has also been shown to be an important RSA feature in plant – plant interaction studies, which have revealed that individuals growing next to each other can sense the presence of neighbours and are able to orient their root development accordingly (de Kroon 2007; Gonkhamdee et al. 2010; Rascher et al. 2011; Faget et al. 2013; Schmid et al. 2015). Because of its complementarity with several root tracing solutions, the use of archiDART can help scientists to choose the most appropriate root image analysis software tool without uniquely focusing on the RSA traits computed by these software packages.

In recent years, root models have become an important tool in root research (Godin and Sinoquet 2005). However, the main limitation in using these models is often the lack of quantitative data. Our R package archiDART can help overcome this issue by providing modellers with useful metrics. Typically, dynamic variables (e.g. growth rates), often used as input parameters in root models (Pagès et al. 2013), can be generated using archiDART. Moreover, density distribution, growth rate and direction can also be used in density-based models (Dupuy et al. 2010).

The functions of the archiDART package have been shown to work efficiently for the computation and analysis of RSA traits of both monocotyledonous (*B. distachyon*) and dicotyledonous plant species (*H. brasiliensis* and *S. lycopersicum*) produced under various growing conditions. Considering that manual, semi-automated and fully automated root tracing solutions offer complementary approaches for the analysis of RSAs, archiDART extends the DART software package and other image analysis tools supporting the RSML format, enabling users to easily calculate a number of RSA traits in a generic data analysis environment for further statistical analyses. As an R

339 package, it has a detailed documentation file for each function and is freely downloadable from the CRAN
340 repository (http://cran.r-project.org/package=archiDART).

341

342 **Conflict of Interest**: The authors declare that they have no conflict of interest.

343

344 **References**

345 Bucksch A, Burridge J, York LM, et al. (2014) Image-based high-throughput field phenotyping of crop roots. Plant
346 Physiol 166:470–486. doi: 10.1104/pp.114.243519

347 Cai J, Zeng Z, Connor JN, et al. (2015) RootGraph : a graphic optimization tool for automated image analysis of
348 plant roots. J Exp Bot. doi: 10.1093/jxb/erv359

349 Clark RT, Famoso AN, Zhao K, et al. (2013) High-throughput two-dimensional root system phenotyping platform
350 facilitates genetic analysis of root growth and development. Plant Cell Environ 36:454–466. doi:
351 10.1111/j.1365-3040.2012.02587.x

352 Clark RT, MacCurdy RB, Jung JK, et al. (2011) Three-dimensional root phenotyping with a novel imaging and
353 software platform. Plant Physiol 156:455–465. doi: 10.1104/pp.110.169102

354 Cobb JN, DeClerck G, Greenberg A, et al. (2013) Next-generation phenotyping : requirements and strategies for
355 enhancing our understanding of genotype-phenotype relationships and its relevance to crop improvement.
356 Theor Appl Genet 126:867–887. doi: 10.1007/s00122-013-2066-0

357 De Dorlodot S, Forster B, Pagès L, et al. (2007) Root system architecture: opportunities and constraints for genetic
358 improvement of crops. Trends Plant Sci 12:474–481. doi: 10.1016/j.tplants.2007.08.012

359 De Kroon H (2007) How do roots interact? Science 318:1562–1563. doi: 10.1126/science.1150726

360 Delaplace P, Delory BM, Baudson C, et al. (2015) Influence of rhizobacterial volatiles on the root system
361 architecture and the production and allocation of biomass in the model grass *Brachypodium distachyon* (L.)
362 P. Beauv. BMC Plant Biol 15:1–15. doi: 10.1186/s12870-015-0585-3

363 Delory BM, Baudson C, Brostaux Y, et al. (2015) archiDART: Plant Root System Architecture Analysis Using
364 DART and RSML Files. R package version 1.1. http://CRAN.R-project.org/package=archiDART.

365 Den Herder G, Van Isterdael G, Beeckman T, De Smet I (2010) The roots of a new green revolution. Trends Plant
366 Sci 15:600–607. doi: 10.1016/j.tplants.2010.08.009

367 Diener J, Nacry P, Périn C, et al. (2013) An automated image-processing pipeline for high-throughput analysis of
368 root architecture in OpenAlea. 7th Int. Conf. Funct. Plant Model. Saariselkä, Finland, pp 85–87

369 Dupuy L, Gregory PJ, Glyn Bengough A (2010) Root growth models: Towards a new generation of continuous
370 approaches. J Exp Bot 61:2131–2143. doi: 10.1093/jxb/erp389

371 Faget M, Nagel KA, Walter A, et al. (2013) Root-root interactions: extending our perspective to be more inclusive
372 of the range of theories in ecology and agriculture using in-vivo analyses. Ann Bot 112:253–266. doi:
373 10.1093/aob/mcs296

374 Fiorani F, Schurr U (2013) Future scenarios for plant phenotyping. Annu Rev Plant Biol 64:267–291. doi:
375 10.1146/annurev-arplant-050312-120137

Forde B, Lorenzo H (2001) The nutritional control of root development. Plant Soil 232:51–68. doi: 10.1023/A:1010329902165

French A, Ubeda-Tomás S, Holman TJ, et al. (2009) High-throughput quantification of root growth using a novel image-analysis tool. Plant Physiol 150:1784–1795. doi: 10.1104/pp.109.140558

Giehl RFH, Gruber BD, von Wirén N (2014) It's time to make changes: modulation of root system architecture by nutrient signals. J Exp Bot 65:769–778. doi: 10.1093/jxb/ert421

Godin C, Sinoquet H (2005) Functional – structural plant modelling. New Phytol 166:705–708.

Gonkhamdee S, Pierret A, Maeght J-L, et al. (2010) Effects of corn (*Zea mays* L.) on the local and overall root development of young rubber tree (*Hevea brasiliensis* Muel. Arg). Plant Soil 334:335–351. doi: 10.1007/s11104-010-0386-2

Iyer-Pascuzzi AS, Symonova O, Mileyko Y, et al. (2010) Imaging and analysis platform for automatic phenotyping and trait ranking of plant root systems. Plant Physiol 152:1148–1157. doi: 10.1104/pp.109.150748

Kumar P, Huang C, Cai J, Miklavcic SJ (2014) Root phenotyping by root tip detection and classification through statistical learning. Plant Soil 380:193–209. doi: 10.1007/s11104-014-2071-3

Le Bot J, Serra V, Fabre J, et al. (2010) DART: a software to analyse root system architecture and development from captured images. Plant Soil 326:261–273. doi: 10.1007/s11104-009-0005-2

Le Marié C, Kirchgessner N, Marschall D, et al. (2014) Rhizoslides : paper-based growth system for non-destructive, high throughput phenotyping of root development by means of image analysis. Plant Methods 10:1–16. doi: 10.1186/1746-4811-10-13

Le Roux Y, Pagès L (1994) Développement et polymorphisme racinaires chez de jeunes semis d'hévéa (*Hevea brasiliensis*). Can J Bot 72:924–932.

Leitner D, Felderer B, Vontobel P, Schnepf A (2014) Recovering root system traits using image analysis exemplified by two-dimensional neutron radiography images of lupine. Plant Physiol 164:24–35. doi: 10.1104/pp.113.227892

Lobet G (2015) rsml: Plant Root System Markup Language (RSML) File Processing. R package version 1.2. http://CRAN.R-project.org/package=rsml.

Lobet G, Draye X, Périlleux C (2013) An online database for plant image analysis software tools. Plant Methods 9:1–7. doi: 10.1186/1746-4811-9-38

Lobet G, Pagès L, Draye X (2011) A novel image-analysis toolbox enabling quantitative analysis of root system architecture. Plant Physiol 157:29–39. doi: 10.1104/pp.111.179895

Lobet G, Pound MP, Diener J, et al. (2015) Root System Markup Language : toward an unified root architecture description language. Plant Physiol 167:617–627. doi: 10.1104/pp.114.253625

López-Bucio J, Cruz-Ramírez A, Herrera-Estrella L (2003) The role of nutrient availability in regulating root architecture. Curr Opin Plant Biol 6:280–287. doi: 10.1016/S1369-5266(03)00035-9

Lynch J (1995) Root architecture and plant productivity. Plant Physiol 109:7–13.

Lynch JP (2013) Steep, cheap and deep: an ideotype to optimize water and N acquisition by maize root systems. Ann Bot 112:347–357. doi: 10.1093/aob/mcs293

Malamy JE (2005) Intrinsic and environmental response pathways that regulate root system architecture. Plant, Cell Environ 28:67–77.

Mathieu L, Lobet G, Tocquin P, Périlleux C (2015) "Rhizoponics": a novel hydroponic rhizotron for root system analyses on mature *Arabidopsis thaliana* plants. Plant Methods 11:1-7. doi: 10.1186/s13007-015-0046-x

Meister R, Rajani MS, Ruzicka D, Schachtman DP (2014) Challenges of modifying root traits in crops for agriculture. Trends Plant Sci 19:779–788. doi: 10.1016/j.tplants.2014.08.005

Nagel KA, Putz A, Gilmer F, et al. (2012) GROWSCREEN-Rhizo is a novel phenotyping robot enabling simultaneous measurements of root and shoot growth for plants grown in soil-filled rhizotrons. Funct Plant Biol 39:891–904.

Pace J, Lee N, Naik HS, et al. (2014) Analysis of maize (*Zea mays* L.) seedling roots with the high-throughput image analysis tool ARIA (Automatic Root Image Analysis). PLoS One 9:e108255. doi: 10.1371/journal.pone.0108255

Pagès L (2014) Branching patterns of root systems: quantitative analysis of the diversity among dicotyledonous species. Ann Bot 114:591–598. doi: 10.1093/aob/mcu145

Pagès L, Bécel C, Boukcim H, et al. (2013) Calibration and evaluation of ArchiSimple, a simple model of root system architecture. Ecol Modell 290:76–84. doi: 10.1016/j.ecolmodel.2013.11.014

Pound MP, French AP, Atkinson JA, et al. (2013) RootNav: navigating images of complex root architectures. Plant Physiol 162:1802–1814. doi: 10.1104/pp.113.221531

R Core Team (2015) R: A language and environment for statistical computing. R Foundation for Statistical Computing, Vienna, Austria. URL http://www.r-project.org/.

Rascher U, Blossfeld S, Fiorani F, et al. (2011) Non-invasive approaches for phenotyping of enhanced performance traits in bean. Funct Plant Biol 38:968–983. doi: 10.1071/FP11164

Rich SM, Watt M (2013) Soil conditions and cereal root system architecture: review and considerations for linking Darwin and Weaver. J Exp Bot 64:1193–1208. doi: 10.1093/jxb/ert043

Schmid C, Bauer S, Bartelheimer M (2015) Should I stay or should I go? Roots segregate in response to competition intensity. Plant Soil 391:283–291. doi: 10.1007/s11104-015-2419-3

Slovak R, Göschl C, Su X, et al. (2014) A scalable open-source pipeline for large-scale root phenotyping of *Arabidopsis*. Plant Cell 26:2390–2403. doi: 10.1105/tpc.114.124032

Thaler P, Pagès L (1996a) Root apical diameter and root elongation rate of rubber seedlings (*Hevea brasiliensis*) show parallel responses to photoassimilate availability. Physiol Plant 97:365–371.

Thaler P, Pagès L (1996b) Periodicity in the development of the root system of young rubber trees (*Hevea brasiliensis* Muell. Arg.): relationship with shoot development. Plant Cell Environ 19:56–64.

Uga Y, Sugimoto K, Ogawa S, et al. (2013) Control of root system architecture by *DEEPER ROOTING 1* increases rice yield under drought conditions. Nat Genet 45:1097–1102. doi: 10.1038/ng.2725

Wells DM, French AP, Naeem A, et al. (2012) Recovering the dynamics of root growth and development using novel image acquisition and analysis methods. Philos Trans R Soc B 367:1517–1524. doi: 10.1098/rstb.2011.0291

Wu J, Pagès L, Wu Q, et al. (2014) Three-dimensional architecture of axile roots of field-grown maize. Plant Soil 387:363–377. doi: 10.1007/s11104-014-2307-2

452 Zhu J, Ingram PA, Benfey PN, Elich T (2011) From lab to field, new approaches to phenotyping root system
453 architecture. Curr Opin Plant Biol 14:310–317. doi: 10.1016/j.pbi.2011.03.020

454

Author's version of the manuscript accepted for publication in *Plant and Soil*
The final publication is available at Springer via http://dx.doi.org/10.1007/s11104-015-2673-4
Delory et al. (2016). *Plant and Soil*, 398, 351-365.

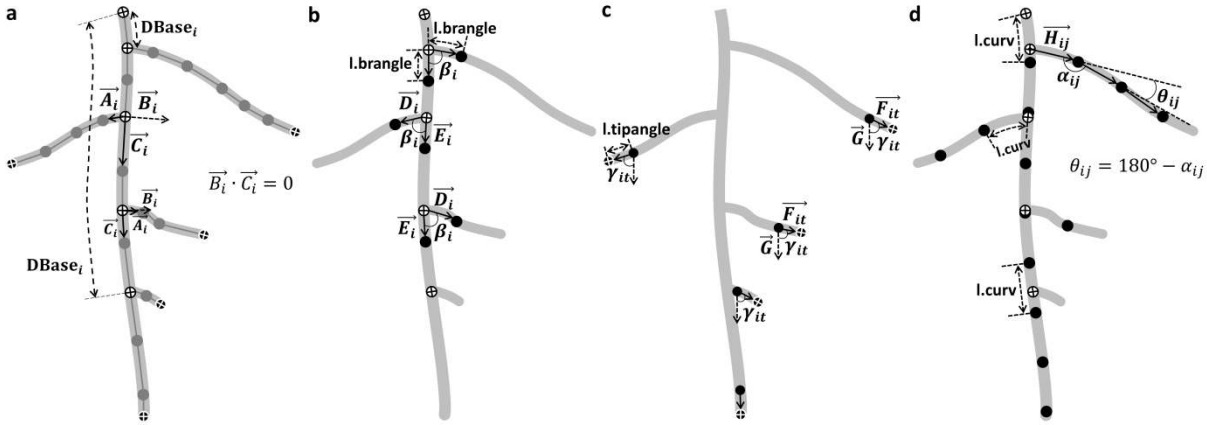

455

456 **Fig. 1 Computation of branching angles (b), root tip angles (c) and root curvatures (d) by *trajectory***. (a) A
457 simple root system after vectorization with a root image analysis software package. In Fig. 1a, the distance between
458 the branching point and the parent root base (referred to as DBase in the text) is shown for two lateral roots. β_i, the
459 branching angle of the root *i* on its corresponding mother root; γ_{it}, the tip angle of the root *i* at the observation date
460 *t*; α_{ij}, the angle *j* between two successive links of the root *i*; θ_{ij}, the angle *j* between the direction vectors of two
461 successive links of the root *i*. White dots with a black cross: branching points; black dots with a white cross: root
462 tips; grey dots: points placed on the root system during the tracing of roots; black dots: new points linearly
463 interpolated by *trajectory*

464

Author's version of the manuscript accepted for publication in *Plant and Soil*
The final publication is available at Springer via http://dx.doi.org/10.1007/s11104-015-2673-4
Delory et al. (2016). *Plant and Soil*, 398, 351-365.

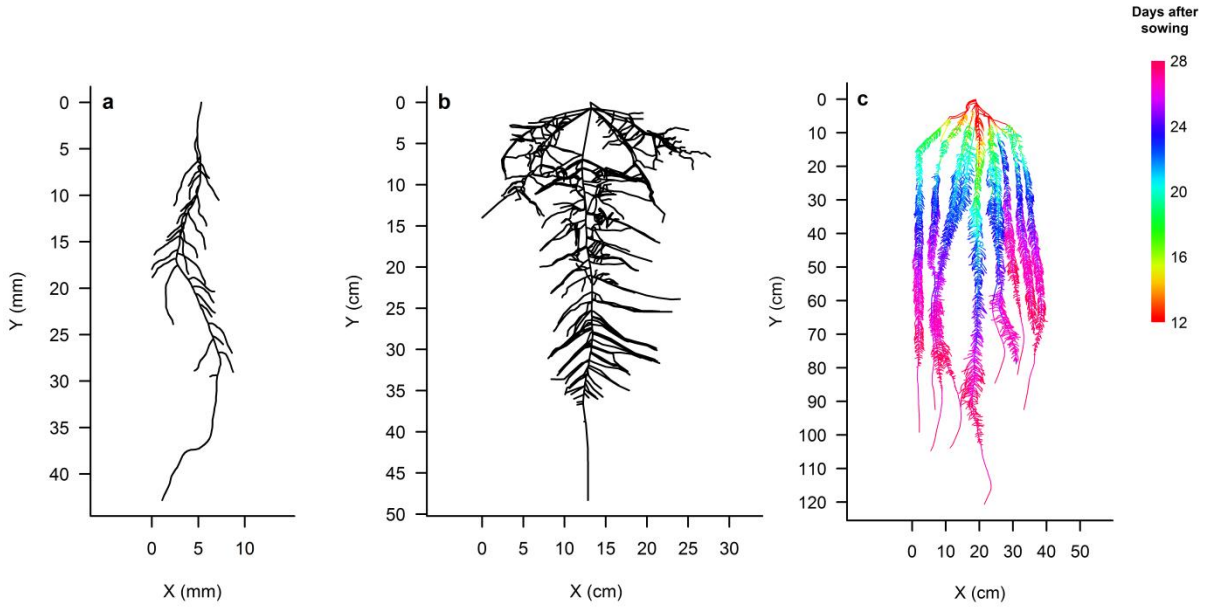

Fig. 2 X-Y plotting of vectorized root systems using *archidraw*. (a) A *B. distachyon* root system produced *in vitro* that was exposed for 11 days to volatiles emitted by *B. subtilis* AP305-GB03, (b) the root system of a 37-day-old *H. brasiliensis* seedling produced in a vertical rhizotron, and (c) part of the root system of a 28-day-old *S. lycopersicum* seedling produced hydroponically in a horizontal flat box. Each root system was plotted at the last observation date. The *S. lycopersicum* root system is shown with a specific colour for each observation date

Author's version of the manuscript accepted for publication in *Plant and Soil*
The final publication is available at Springer via http://dx.doi.org/10.1007/s11104-015-2673-4
Delory et al. (2016). *Plant and Soil*, 398, 351-365.

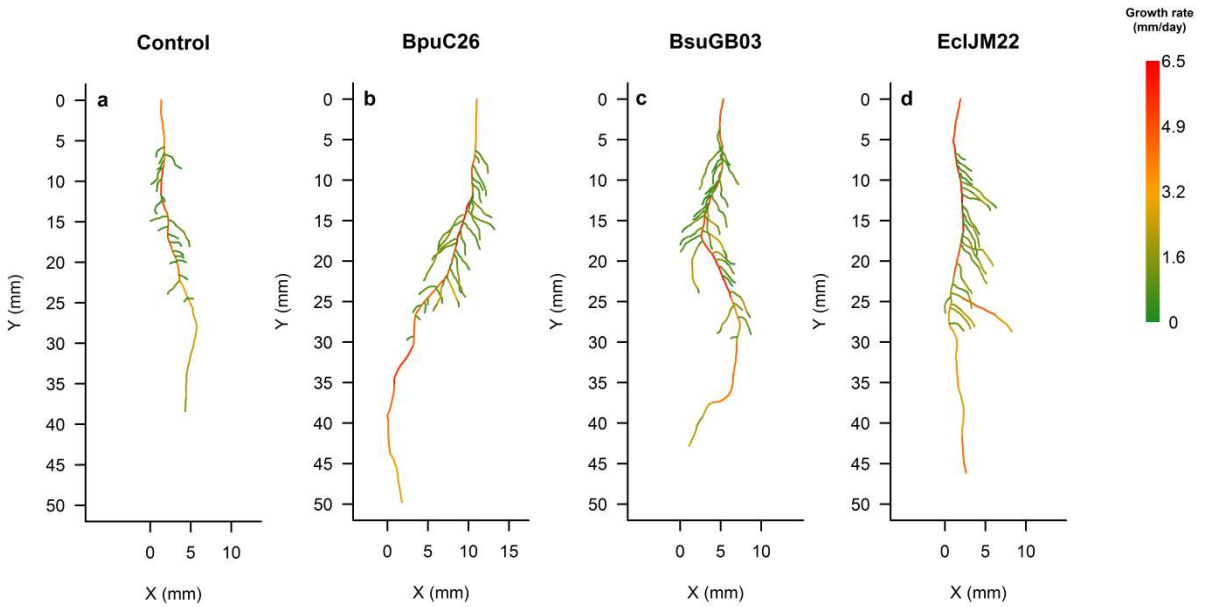

Fig. 3 X-Y plotting of vectorized *B. distachyon* root systems using *archigrow*. Plants were either cultivated without PGPR (control) or exposed to volatiles emitted by *B. pumilus* C26 (BpuC26), *B. subtilis* AP305-GB03 (BsuGB03) or *E. cloaceae* AP12-JM22 (EclJM22) for 11 days. Each root system was plotted at the last observation date. The colour code used for each link depends on its corresponding growth rate value and is shown at the right side of the plot

Author's version of the manuscript accepted for publication in *Plant and Soil*
The final publication is available at Springer via http://dx.doi.org/10.1007/s11104-015-2673-4
Delory et al. (2016). *Plant and Soil*, 398, 351-365.

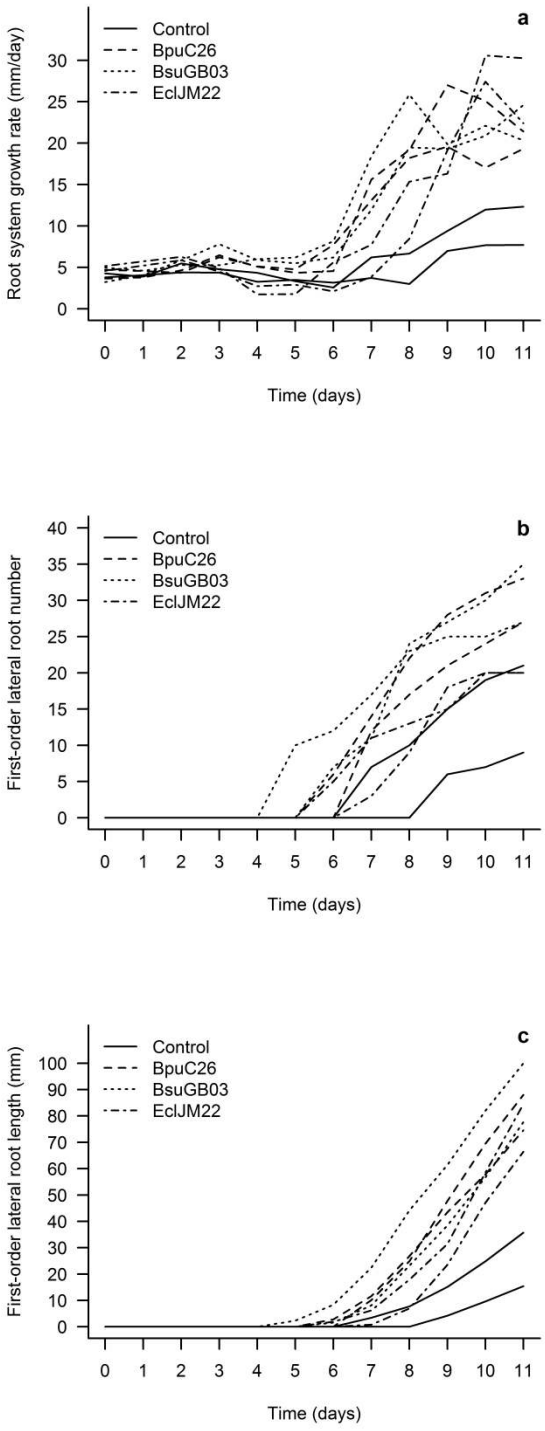

Fig. 4 Evolution of the root system growth rate (a), the first-order lateral root number (b), and the first-order lateral root length (c) of representative *B. distachyon* plantlets co-cultivated or not with PGPR. Plants were either cultivated without PGPR (control) or exposed to volatiles emitted by *B. pumilus* C26 (BpuC26), *B. subtilis* AP305-GB03 (BsuGB03) or *E. cloaceae* AP12-JM22 (EclJM22) for 11 days. RSA parameters were calculated using the function *architect*

Author's version of the manuscript accepted for publication in *Plant and Soil*
The final publication is available at Springer via http://dx.doi.org/10.1007/s11104-015-2673-4
Delory et al. (2016). *Plant and Soil*, 398, 351-365.

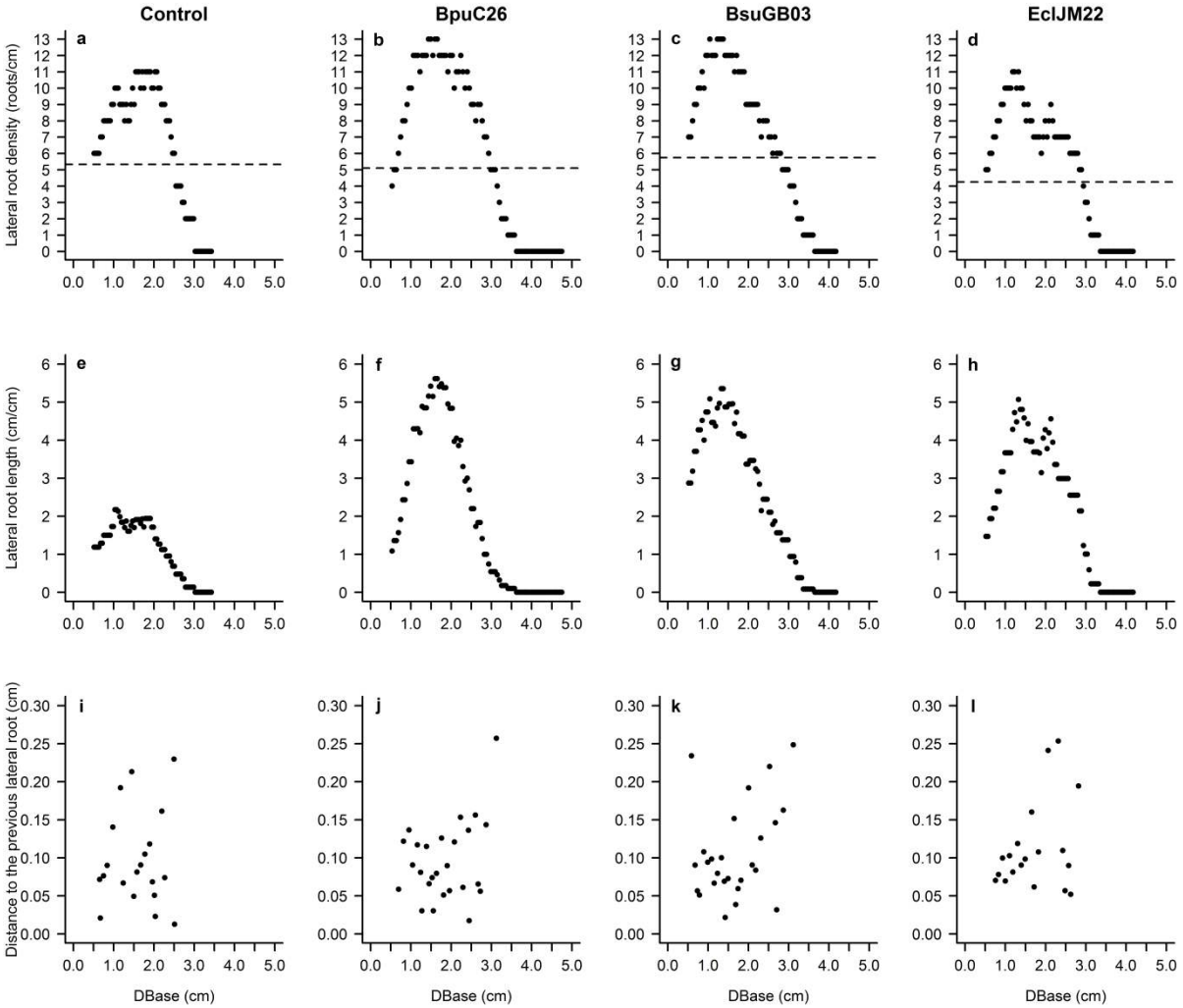

Fig. 5 Analysis of the first-order lateral root density distribution (a-d), the first-order lateral root length distribution (e-h) and the inter-branch distance between neighbouring first-order lateral roots (i-l) on the primary root of representative *B. distachyon* plantlets co-cultivated or not with PGPR. Plants were either cultivated without PGPR (control) or exposed to volatiles emitted by *B. pumilus* C26 (BpuC26), *B. subtilis* AP305-GB03 (BsuGB03) or *E. cloaceae* AP12-JM22 (EclJM22) for 11 days. DBase refers to the distance between the branching point of a first-order lateral root to the parent root base. Each horizontal dashed line refers to the mean secondary root density calculated by *latdist* along each primary root (Control: 5.3 roots/cm; BpuC26: 5.1 roots/cm; BsuGB03: 5.7 roots/cm; EclJM22: 4.3 roots/cm). Calculations were performed using the function *latdist* with an interval length of 1 cm and an interpolation value of 100

Author's version of the manuscript accepted for publication in *Plant and Soil*
The final publication is available at Springer via http://dx.doi.org/10.1007/s11104-015-2673-4
Delory et al. (2016). *Plant and Soil*, 398, 351-365.

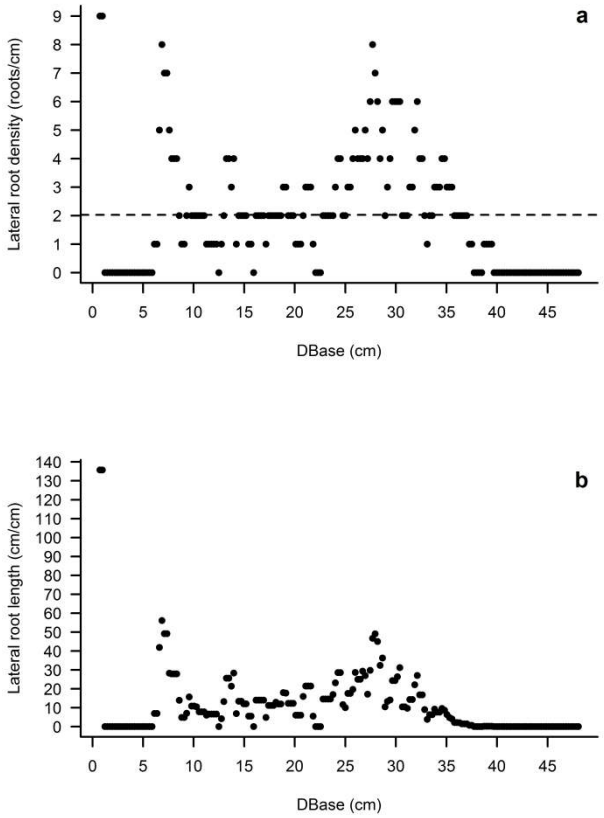

Fig. 6 Analysis of the first-order lateral root density distribution (a) and the first-order lateral root length distribution (b) along the taproot of a 37-day-old *H. brasiliensis* root system produced in a vertical rhizotron. DBase refers to the distance between the branching point of a first-order lateral root to the parent root base. The horizontal dashed line refers to the mean secondary root density calculated by *latdist* along the taproot (2.0 roots/cm)

Author's version of the manuscript accepted for publication in *Plant and Soil*
The final publication is available at Springer via http://dx.doi.org/10.1007/s11104-015-2673-4
Delory et al. (2016). *Plant and Soil*, 398, 351-365.

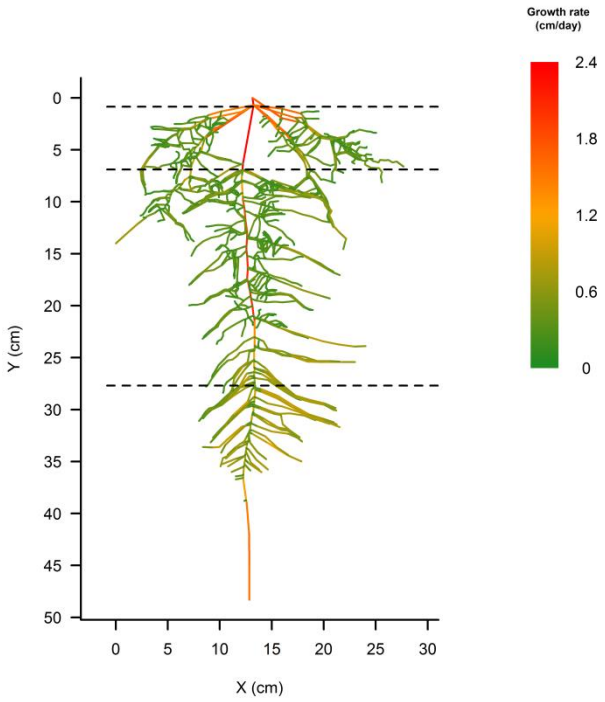

503

504 **Fig. 7 X-Y plotting of a 37-day-old *H. brasiliensis* root system produced in a vertical rhizotron using**
505 ***archigrow*.** The root system was plotted at the last observation date. The colour code used for each link depends
506 on its corresponding growth rate value and is shown at the right side of the plot. Regions of the taproot associated
507 with high first-order lateral root densities are located at the intersection of the taproot and each horizontal dashed
508 line

509

Author's version of the manuscript accepted for publication in *Plant and Soil*
The final publication is available at Springer via http://dx.doi.org/10.1007/s11104-015-2673-4
Delory et al. (2016). *Plant and Soil*, 398, 351-365.

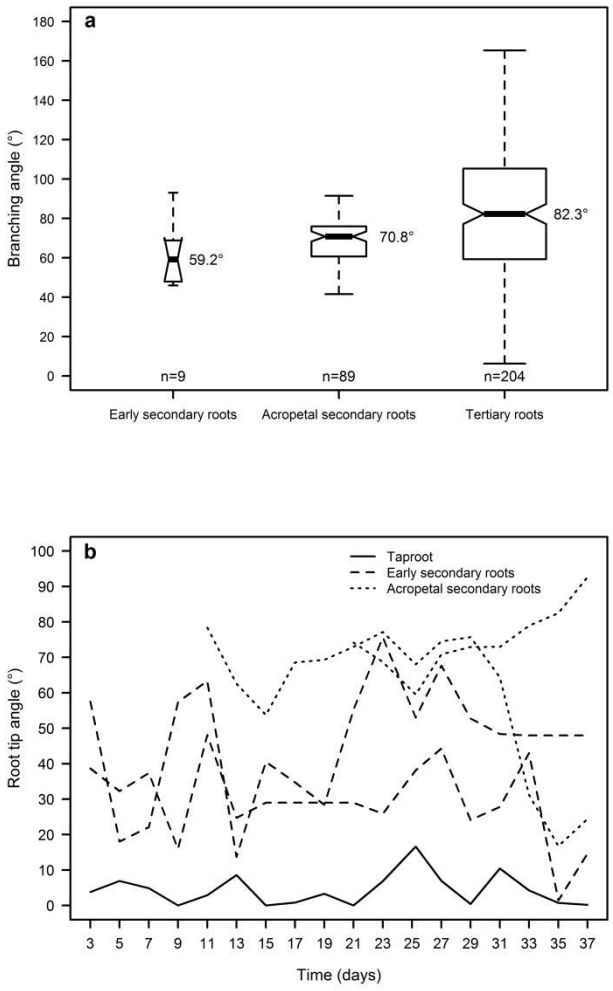

510

511 **Fig. 8 Analysis of the branching angles (a) and the gravitropism (b) of selected roots of a 37-day-old *H.***
512 ***brasiliensis* root system produced in a vertical rhizotron.** In Figure a, the branching angles were calculated
513 separately for the main root types identified by Le Roux and Pagès (1994). In each boxplot, the whiskers were
514 extended to the most extreme data points localized between the hinges of the box and 1.5 times the interquartile
515 range. For clarity reasons, Figure b shows only the evolution of the root tip angle for the taproot, the two longest
516 early secondary roots and the two longest acropetal secondary roots. Calculations were performed using the
517 *trajectory* function with the l.brangle and l.tipangle set at 0.5 cm

518

Author's version of the manuscript accepted for publication in *Plant and Soil*
The final publication is available at Springer via http://dx.doi.org/10.1007/s11104-015-2673-4
Delory et al. (2016). *Plant and Soil*, 398, 351-365.

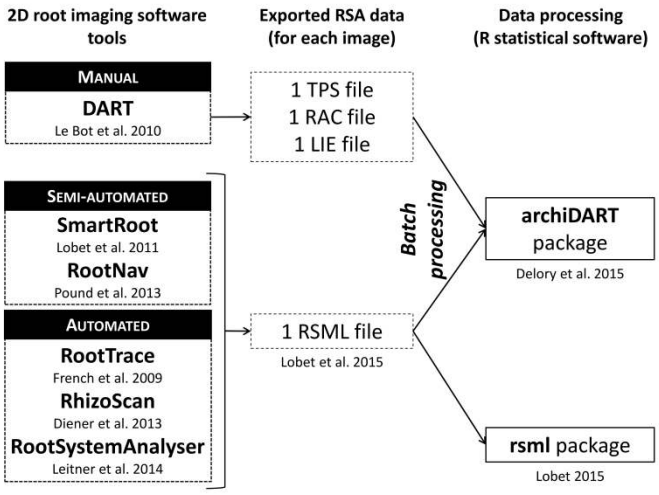

519

520 **Fig. 9 Root system architecture analysis pipeline: from data acquisition to data processing**

Author's version of the manuscript accepted for publication in *Plant and Soil*
The final publication is available at Springer via http://dx.doi.org/10.1007/s11104-015-2673-4
Delory et al. (2016). *Plant and Soil*, 398, 351-365.

Table 1 Overview of the required files, returned R objects and calculated RSA traits for each R function of the archiDART package (version 1.1). DART, Data Analysis of Root Tracings; RAC, DART-generated file storing topological and length attributes for each individual root of a vectorized root system (file extension: .rac); TPS, DART-generated file storing temporal attributes for each observation date (file extension: .tps); LIE, DART-generated file storing spatial attributes for each point used to construct a vectorized root system (file extension: .lie); RSML, Root System Markup Language; UT, the unit of time used by the experimenter; mm, millimetres; cm, centimetres; px, pixels; d, degrees; r, radians

R function	DART/RSML files	Returned R objects	RSA traits	Units
archidraw	LIE RSML	Plot window	×	×
archigrow	LIE + TPS	Plot window List	× Individual root growth rate at each observation date	× (mm, cm or px)/UT
architect	RAC + TPS RSML	Data frame	*For each observation date:* Length of the root system Growth rate of the root system Length of the first-order root[a] Growth rate of the first-order root[a] Total number of lateral roots Total length of lateral roots Total number of lateral roots by branching order Total length of lateral roots by branching order Mean length of lateral roots by branching order Growth rate of lateral roots by branching order Density of secondary roots on the first-order root[a] Secondary root number distribution on the first-order root[a] Secondary root length distribution on the first-order root[a] Secondary root density distribution on the first-order root[a]	 mm, cm or px (mm, cm or px) /UT mm, cm or px (mm, cm or px) /UT - mm, cm or px - mm, cm or px mm, cm or px (mm, cm or px) /UT mm^{-1}, cm^{-1} or px^{-1} - mm, cm or px mm^{-1}, cm^{-1} or px^{-1}
latdist	RAC RSML	List	*For each mother root:* Total number of lateral roots Mean lateral root density Lateral root density distribution Lateral root length distribution Distance to the previous lateral root (inter-branch distance)	 - mm^{-1}, cm^{-1} or px^{-1} mm^{-1}, cm^{-1} or px^{-1} mm/mm, cm/cm or px/px mm, cm or px
trajectory	RAC + LIE + TPS RSML	List	Tortuosity Orientation Branching angle of each daughter root on its corresponding mother root The mean and the standard deviation of the local angle values calculated between the direction vectors of the successive links constructed using equidistantly spaced interpolated points along each root of a vectorized root system *For each observation date:* Root tip angle relative to a vertical direction vector	- - d or r d or r d or r

[a] When analysing the topology of a root system, a first-order root is defined as a root that is directly connected to the shoot.

Author's version of the manuscript accepted for publication in *Plant and Soil*
The final publication is available at Springer via http://dx.doi.org/10.1007/s11104-015-2673-4
Delory et al. (2016). *Plant and Soil*, 398, 351-365.

530 **Table 2 Description of the RSA traits computed by the functions of the R package archiDART (version**
531 **1.1)**

RSA traits	Description
Root length	The length of a root is calculated as the length of the polyline (i.e. a succession of linear segments) constituting the skeletonized root. Root length calculations are performed using the spatial and topological information exported from DART or using the geometry elements (SCENE > PLANT > ROOT > Geometry > polyline) stored in each RSML file.
Root number	The number of root elements constituting a skeletonized root system.
Root growth rate	For the first observation date, it is calculated as the ratio of the root length to the root system age. For other observation dates (t), it is calculated as the difference between the root length at time t and t-1 divided by the difference between the root system age at time t and t-1.
Lateral root density	For each mother root, it is calculated as the total number of daughter roots directly connected to the parent root divided by the length of the mother root. When evaluating the lateral root density distribution, the *latdist* function calculates local lateral root densities at intervals of a length defined by the experimenter and centred on points located at various distances from the parent root base.
Inter-branch distance	The distance separating a lateral root from its closest neighbour located at the greatest distance from the apex of the mother root.
Tortuosity	The ratio of the root length to the Euclidean distance between the root base and the apex.
Orientation (Fig. 1a)	Does a daughter root emerge at the left ($\overrightarrow{A_i} \cdot \overrightarrow{B_i} > 0$) or the right ($\overrightarrow{A_i} \cdot \overrightarrow{B_i} < 0$) side of the parent root? $\overrightarrow{A_i}$ is a direction vector going from the branching point to the following point on the daughter root *i*. $\overrightarrow{B_i}$ is a vector orthogonal to a direction vector going the branching point to the following point on the mother root of the root *i*. In this paper, we consider that the normal vector that is orthogonal to a direction vector (a,b) will have the following coordinates: (b,-a).
Branching angle (Fig. 1b)	The branching angle β_i of the root *i* on its parent root is calculated according to the following equation: $$\beta_i = \cos^{-1}\left(\frac{\left\|\overrightarrow{D_i} \cdot \overrightarrow{E_i}\right\|}{\left\|\overrightarrow{D_i}\right\| \cdot \left\|\overrightarrow{E_i}\right\|}\right)$$ $\overrightarrow{D_i}$ is a direction vector going from the branching point to a linearly interpolated point located at a user-specified distance (l.brangle) from the branching point on the daughter root *i*. $\overrightarrow{E_i}$ is a direction vector going from the branching point to a linearly interpolated point located at a user-specified distance (l.brangle) from the branching point on the parent root of the root *i*.
Root tip angle (Fig. 1c)	The tip angle γ_{it} of the root *i* at the observation date *t* is calculated according to the following equation: $$\gamma_{it} = \cos^{-1}\left(\frac{\left|\overrightarrow{F_{it}} \cdot \vec{G}\right|}{\left\|\overrightarrow{F_{it}}\right\| \cdot \left\|\vec{G}\right\|}\right)$$ $\overrightarrow{F_{it}}$ is a direction vector going from a linearly interpolated point placed along the root *i* at a user-defined distance from the apex (l.tipangle) to the root tip. $\vec{G}$ is a vertical direction vector.
Root curvature (Fig. 1d)	The curvature of the root *i* is evaluated by statistical parameters (mean and standard deviation) describing the distribution of local angles (θ_{ij}) measured along each root following the method proposed by French et al. (2009).

532